Hierarchical Management of Distributed Energy Resources Using Chance-Constrained OPF and Extremum Seeking Control

Preprint

Yue Chen and Yashen Lin

National Renewable Energy Laboratory

Presented at the American Control Conference
Philadelphia, Pennsylvania
July 10–12, 2019

NREL is a national laboratory of the U.S. Department of Energy
Office of Energy Efficiency & Renewable Energy
Operated by the Alliance for Sustainable Energy, LLC

This report is available at no cost from the National Renewable Energy Laboratory (NREL) at www.nrel.gov/publications.

Contract No. DE-AC36-08GO28308

Conference Paper
NREL/CP-5D00-73404
June 2019

Hierarchical Management of Distributed Energy Resources Using Chance-Constrained OPF and Extremum Seeking Control

Preprint

Yue Chen and Yashen Lin

National Renewable Energy Laboratory

Suggested Citation
Chen, Yue, and Yashen Lin. 2019. *Hierarchical Management of Distributed Energy Resources Using Chance-Constrained OPF and Extremum Seeking Control: Preprint*. Golden, CO: National Renewable Energy Laboratory. NREL/CP-5D00-73404. https://www.nrel.gov/docs/fy19osti/73404.pdf.

Contract No. DE-AC36-08GO28308

Conference Paper
NREL/CP-5D00-73404
June 2019

National Renewable Energy Laboratory
15013 Denver West Parkway
Golden, CO 80401
303-275-3000 • www.nrel.gov

NOTICE

This work was authored by the National Renewable Energy Laboratory, operated by Alliance for Sustainable Energy, LLC, for the U.S. Department of Energy (DOE) under Contract No. DE-AC36-08GO28308. Funding provided by U.S. Department of Energy Office of Electricity Delivery and Energy Reliability. The views expressed herein do not necessarily represent the views of the DOE or the U.S. Government. The U.S. Government retains and the publisher, by accepting the article for publication, acknowledges that the U.S. Government retains a nonexclusive, paid-up, irrevocable, worldwide license to publish or reproduce the published form of this work, or allow others to do so, for U.S. Government purposes.

Cover Photos by Dennis Schroeder: (clockwise, left to right) NREL 51934, NREL 45897, NREL 42160, NREL 45891, NREL 48097, NREL 46526.

Hierarchical Management of Distributed Energy Resources Using Chance-Constrained OPF and Extremum Seeking Control

Yue Chen, Yashen Lin

***Abstract*— Distributed energy resources (DERs) are becoming an important part of distribution systems, because of their economic and environmental benefits. Although their inherent intermittency and volatility introduce uncertainties into the electric power system, they have the potential to provide controllability to the system under proper coordination. In this paper, we propose a hierarchical control algorithm for distribution systems with DERs so that they have controllability similar to a generator bus. The upper level scheduler solves a chance-constrained optimal power flow (OPF) problem to plan the operation of the DERs based on forecasts, and the lower level distributed DER controllers leverage the extremum seeking approach to deliver the planned power at the feeder head. The proposed algorithm is tested on a modified IEEE 13-node feeder, demonstrating its effectiveness.**

I. Introduction

Increasing integration of distributed energy resources (DERs) provides multiple challenges and opportunities to improve the reliability, resilience, and cost-effectiveness of future electric grid operations [1], [2]. Traditionally, transmission system operators view generator buses as primary controllability providers and DERs as sources of uncertainty. Properly coordinated DERs in the distribution systems, however, have the potential to make the load buses a major player in providing the controllability system operators need.

In this paper, we propose a hierarchical control algorithm for distribution systems with DERs. The overall objective is to control the DERs, so that the power injection at the distribution system feeder head can be scheduled, similar to a generator bus. This is achieved by an upper level scheduler that plans the operation of the DERs based on the forecast and the lower level real-time controllers that deliver the planned power at the feeder head. One challenge in achieving this objective is handling the uncertainties in the distribution system. This is addressed at both control levels. The upper level scheduler solves a chance-constrained optimal power flow (OPF) problem, which ensures there is enough reserve to compensate for the uncertainties. The chance constraints are reformulated into deterministic form, and the OPF can be reformulated as a second-order cone programming problem, which can be solved efficiently by established solvers. The scheduler is updated regularlyunder the model predictive control (MPC) framework to further improve robustness. In the lower level real-time control, the extremum seeking (ES) control is adopted [3]. This lower level control uses DER reserve in response to noise to maintain the scheduled feeder head power.

Substantial work has been done to operating distribution systems with DERs. OPF is a fundamental tool for planning and operation [4], [5]. A variety of OPF approaches have been proposed to account for uncertainties, which include robust- and scenario- based method [6], multistage stochastic programming techniques [7], and chance-constrained formulations [8]–[12].

In this paper, we adopt the chance-constrained formulation, which provides an intuitive way to quantify the system security level. In addition to the common objective of minimizing the operating cost with a certain level of reserve, we introduce the noise distribution factor as a control variable to optimally specify each DER's responsibility to handle system uncertainty. Another highlight of the proposed chance-constrained OPF formulation is that it considers both the spatial and temporal correlations of bus noise.

The distributed control algorithm for DERs has been studied in a number of research works, for example, [13]–[15]. Many studies focus on voltage control. In this paper, we adopt the ES control algorithm [3]. The algorithm can be leveraged to modulate the power output of DERs to minimize the difference between the delivered power and a reference signal at the feeder head [16]. This naturally fits the proposed hierarchical control algorithm so that the scheduler can provide the power reference signal for the DERs to track using the distributed ES controllers.

Overall, the main contributions of this paper are: (i) we propose a hierarchical control algorithm for distribution systems with DERs so that they have controllability similar to generator buses; and (ii) we develop a chance-constrained OPF for the upper level scheduling problem, which considers both spatial and temporal correlation among the noises at different buses and times.

The rest of the paper is organized as follows. Section II provides an overview of the hierarchical control algorithm. Section III and IV describe the upper level scheduler and the lower level real-time ES controllers, respectively. Section V discusses connecting the two control levels. Section VI presents the simulation results. Section VII concludes the paper and discusses future work.

*This work was authored by the National Renewable Energy Laboratory, operated by Alliance for Sustainable Energy, LLC, for the U.S. Department of Energy (DOE) under Contract No. DE-AC36-08GO28308. Funding provided by U.S. Department of Energy Office of Electricity Delivery and Energy Reliability. The views expressed in the article do not necessarily represent the views of the DOE or the U.S. Government. The U.S. Government retains and the publisher, by accepting the article for publication, acknowledges that the U.S. Government retains a nonexclusive, paid-up, irrevocable, worldwide license to publish or reproduce the published form of this work, or allow others to do so, for U.S. Government purposes.

Y. Chen and Y. Lin are with the Power Systems Engineering Center, National Renewable Energy Laboratory, Golden, CO 80401, USA {yue.chen, yashen.lin}@nrel.gov

II. Hierarchical control

A schematic of the proposed hierarchical control algorithm is shown in Fig. 1. The upper level scheduler solves a chance-constrained OPF for a multi-hour look-ahead horizon with time steps in minutes. The set points for the DERs, as well as the scheduled feeder head power injection, are passed to the lower level real-time controller, which operates in the seconds timescale. The ES control algorithm is implemented at the DERs, which uses the actual feeder head power measurement to adjust its power output, so that the scheduled power reference signal can be tracked at the feeder head. To increase the robustness of the proposed algorithm, we adopted the MPC framework, where the DER states and forecasts are updated regularly in the upper level scheduler.

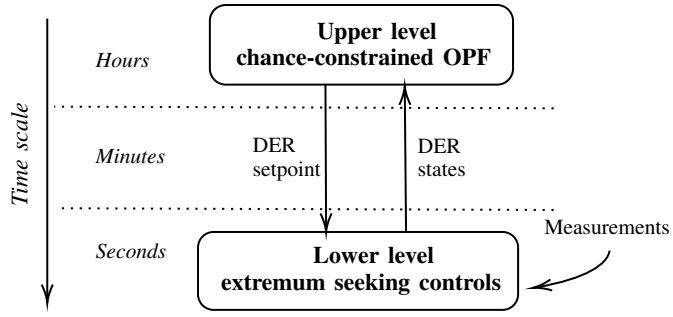

Fig. 1. Schematic of the proposed hierarchical control.

III. Upper Level Scheduler

In this section, we describe the upper level scheduler, which solves a chance-constrained OPF problem. The idea is to minimize cost while reserving a certain capacity from the energy storage devices to compensate for the uncertainty that occurs at the load and PV buses. For the rest of the paper, we denote τ as the time index at the upper level and t as the time index at the lower level.

A. Objective Function

Let $P_{1,\tau}$ denote the power at the feeder head, and let $c_{p,\tau}$ denote the electricity price in time horizon τ. We consider the following objective function:

$$J = \sum_{\tau=1}^{\mathcal{T}} c_{p,\tau} P_{1,\tau} \Delta\tau + \bar{c}_p \sum_i (SOC_{i,0} - SOC_{i,\mathcal{T}}) \quad (1)$$

where $\bar{c}_p$ is the average electricity price, $\Delta\tau$ is the length of time in one horizon, $SOC_{i,\tau}$ represents the state of charge (SOC) for storage i at time τ, and $SOC_{i,0}$ is the initial SOC. The first term in (1) captures the electricity cost of the distribution system, and the second term captures the cost of energy storages.

B. Constraints

1) Energy storage limits: The energy storage limits are formulated as chance constraints so that there is sufficient reserve to compensate the uncertainty with a predetermined probability. To represent the uncertainty, a random variable $w_{i,\tau}$ is defined as the power noise injected into node i, in time horizon τ. The uncertainties are both spatially and temporally correlated, and we assume all uncertainties are zero-mean multivariate Gaussian. More details on uncertainty noise modeling are provided in Section III-E.

Ignoring power loss, the total uncertainty in the system $w_{\Sigma,\tau}$ can be written as:

$$w_{\Sigma,\tau} = \sum_i w_{i,\tau} \quad (2)$$

To ensure good system performance under uncertainties, energy storage devices are used to handle $w_{\Sigma,\tau}$. Let U_b be the power from energy storage devices to correct the noise. For node i, we have:

$$U_{b,i,\tau} = -\alpha_{i,\tau} w_{\Sigma,\tau}, \text{ where} \sum_i \alpha_{i,\tau} = 1, \alpha_{i,\tau} \geq 0 \quad (3)$$

The factor α_i specifies the portion of total uncertainty handled by the energy storage at node i.

Let $U_{i,\tau}$ be the real power injection from the energy storage at node i. The chance constraints for the power limits of the energy storage can be written as:

$$\mathbf{P}\left(U_{i,\tau} + U_{b,i,\tau} \leq U_i^{max}\right) \geq \gamma \quad (4a)$$
$$\mathbf{P}\left(U_{i,\tau} + U_{b,i,\tau} \geq U_i^{min}\right) \geq \gamma \quad (4b)$$

Next, we impose chance constraints on the SOC limits of the energy storage:

$$\mathbf{P}\left(SOC_{i,\tau} \leq SOC_i^{max}\right) \geq \gamma \quad (5a)$$
$$\mathbf{P}\left(SOC_{i,\tau} \geq SOC_i^{min}\right) \geq \gamma \quad (5b)$$

The SOC can be expressed as:

$$SOC_{i,\tau} = SOC_{i,0} + \sum_{k=1}^{\tau} \left(-U_{i,k} + \alpha_{i,k} w_{\Sigma,k}\right) \Delta\tau \quad (6)$$

These chance constraints can be reformulated as a deterministic form under the Gaussian noise assumption. This is discussed in Section III-C.

2) Power flow constraints: Consider a radial distribution system that is described by a node set $\mathcal{B}$ and a line segment set $\mathcal{L}$. The set $\mathcal{B} = \{1, \ldots, n\}$ denotes total n nodes, where node 1 denotes the feeder head, which has a fixed voltage and flexible real and reactive power. Each element in set $\mathcal{L}$ is a node pair (i, j) that represents a line with power flowing from node i to node j.

We adopt the *DistFlow* developed by Baran and Wu [17]. Because there is no time coupling, we drop the time index τ in this subsection for the convenience of notation. At node i, let P_i and Q_i be the real and reactive branch power injection, $P_{l,i}$ and $Q_{l,i}$ be the real and reactive load demand, $P_{pv,i}$ and $Q_{pv,i}$ be the real and reactive PV generation, U_i be the real power injection from energy storage, v_i be the squared voltage magnitude, and $Z_{ij} = R_{ij} + jX_{ij}$ be the impedance of line (i, j). For any $(i, j) \in \mathcal{L}$, the branch flow equations

can be written as:

$$P_i = P_{l,i} - P_{pv,i} - U_i - U_{b,i} + w_i + \sum_{j:(i,j)\in\mathcal{L}} (P_j + R_{ij} l_{ij}) \tag{7a}$$

$$Q_i = Q_{l,i} - Q_{pv,i} + \sum_{j:(i,j)\in\mathcal{L}} (Q_j + X_{ij} l_{ij}) \tag{7b}$$

$$v_i = v_j + 2(R_{ij}P_j + X_{ij}Q_j) + (R_{ij}^2 + X_{ij}^2) l_{ij} \tag{7c}$$

$$l_{ij} = \frac{P_j^2 + Q_j^2}{v_j} \tag{7d}$$

The power flow equations (7) are nonlinear through the term l_{ij} in (7d). It is linearized by using the first-order Taylor series expansion at nominal values $\{P_{j,0},\, Q_{j,0},\, v_{j,0}\}$:

$$\frac{P_j^2 + Q_j^2}{v_j} \approx c_p P_j + c_q Q_j + c_v v_j \tag{8}$$

where, coefficients are determined as $c_p = 2\frac{P_{j,0}}{v_{j,0}}$, $c_q = 2\frac{Q_{j,0}}{v_{j,0}}$, and $c_v = -\frac{P_{j,0}^2+Q_{j,0}^2}{v_{j,0}^2}$.

3) Voltage limits: In general form, the voltage limits can be written as:

$$v_i^{min} \le v_i \le v_i^{max}, \quad i = 1, \ldots, n$$

Although the actual node voltage is affected by the noises through the term $(-U_{b,i} + w_i)$, this term is small compare to others in (7a). Therefore, we neglect the contribution of the noises to the node voltages.

C. Deterministic Reformulation of Chance Constraints

The following technique is used to reformulate the chance constraints as deterministic constraints, so that the optimization problem can be efficiently solved. This deterministic reformulation is also seen in related works [8]–[12].

Consider a general chance constraint:

$$\mathbf{P}\left(a^T x \le b\right) \ge \gamma \tag{9}$$

where γ is the required reliable probability, and a is a multivariate Gaussian random variable, i.e., $a \sim \mathcal{N}(\bar{a}, \Sigma)$. From the property of Gaussian distribution, we have:

$$\mathbf{P}\left(a^T x \le b\right) = \Phi\left(\frac{b - \bar{a}^T x}{\sqrt{x^T \Sigma x}}\right) \tag{10}$$

where, Φ is the cumulative density function of the standard normal distribution $N(0,1)$. Eq. (9) can then be written in a deterministic form:

$$b - \bar{a}^T x \ge \Phi^{-1}(\gamma)\, ||\Sigma^{\frac{1}{2}} x||_2 \tag{11}$$

Note that the constraint (11) is a linear constraint when x is known and a second-order cone constraint when x is a decision variable and $\gamma \ge 0.5$.

With this technique, the chance constraints (4) can be reformulated as the following deterministic constraints:

$$U_{i,\tau} \le U_i^{max} - \Phi^{-1}(\gamma)\sigma\alpha_{i,\tau} \tag{12a}$$

$$U_{i,\tau} \ge U_i^{min} + \Phi^{-1}(\gamma)\sigma\alpha_{i,\tau} \tag{12b}$$

where σ is the standard deviation of the aggregate noise $w_{\Sigma,\tau}$.

Similarly, we can reformulate the chance constraints for the SOC (5) into deterministic form. The time series $\{w_{\Sigma,\tau},\ \tau=1,\ldots,T\}$ is temporally correlated. Denote the auto-covariance matrix of the vector $[w_{\Sigma,1}, \cdots, w_{\Sigma,\tau}]$ by Σ_τ. In addition, let vector $\boldsymbol{\alpha}_{i,\tau}^{time}$ collects the time series of α for node i up to time horizon τ, i.e., $\boldsymbol{\alpha}_{i,\tau}^{time} = [\alpha_{i,1}, \cdots, \alpha_{i,\tau}]$. Note that the dimension of both $\boldsymbol{\alpha}_{i,\tau}^{time}$ and Σ_τ grows as time advances. Applying the chance constraint reformulation (11), we obtain the following constraints on SOC: for the energy storage at node i:

$$U_{\Sigma,i,\tau}\Delta t \ge SOC_{i,0} - SOC_i^{max} + \Phi^{-1}(\gamma)||\Sigma_\tau^{\frac{1}{2}}\boldsymbol{\alpha}_{i,\tau}^{time}||_2\Delta\tau$$

$$U_{\Sigma,i,\tau}\Delta t \le SOC_{i,0} - SOC_i^{min} - \Phi^{-1}(\gamma)||\Sigma_\tau^{\frac{1}{2}}\boldsymbol{\alpha}_{i,\tau}^{time}||_2\Delta\tau$$

where $U_{\Sigma,i,\tau} = U_{i,1} + \cdots + U_{i,\tau}$. The computation of Σ_τ is postponed to Section III-E.

D. Reformulated Optimal Power Flow

The finite-horizon scheduling problem can now be formulated as the following second-order cone programming:

$$\underset{\boldsymbol{U},\boldsymbol{\alpha}}{\text{Minimize}} \sum_{\tau=\mathcal{T}_1}^{\mathcal{T}_1+\mathcal{T}-1} c_{p,\tau} P_{1,\tau}\Delta\tau + \bar{c}_p \sum_i \Delta SOC_i \tag{14a}$$

Subject to

$$P_{i,\tau} = P_{l,i,\tau} - P_{pv,i,\tau} - U_{i,\tau} + \sum_{j:(i,j)\in\mathcal{L}} (P_{j,\tau} + R_{ij} l_{ij,\tau}) \tag{14b}$$

$$Q_{i,\tau} = Q_{l,i,\tau} - Q_{pv,i,\tau} + \sum_{j:(i,j)\in\mathcal{L}} (Q_{j,}\tau + X_{ij} l_{ij,\tau}) \tag{14c}$$

$$v_{i,\tau} = v_j + 2(R_{ij}P_{j,\tau} + X_{ij}Q_j) + (R_{ij}^2 + X_{ij}^2) l_{ij,\tau} \tag{14d}$$

$$l_{ij,\tau} = c_p P_{j,\tau} + c_q Q_{j,\tau} + c_v v_{j,\tau},\ (i,j) \in \mathcal{L} \tag{14e}$$

$$U_{i,\tau} \le U_i^{max} - \Phi^{-1}(\gamma)\sigma\alpha_{i,\tau} \tag{14f}$$

$$U_{i,\tau} \ge U_i^{min} + \Phi^{-1}(\gamma)\sigma\alpha_{i,\tau} \tag{14g}$$

$$U_{\Sigma,i,\tau}\Delta\tau \ge SOC_{i,\mathcal{T}_1} - SOC_i^{max} + \Phi^{-1}(\gamma)||\Sigma_\tau^{\frac{1}{2}}\boldsymbol{\alpha}_{i,\tau}^{time}||_2\Delta\tau \tag{14h}$$

$$U_{\Sigma,i,\tau}\Delta\tau \le SOC_{i,\mathcal{T}_1} - SOC_i^{min} - \Phi^{-1}(\gamma)||\Sigma_\tau^{\frac{1}{2}}\boldsymbol{\alpha}_{i,\tau}^{time}||_2\Delta\tau \tag{14i}$$

$$v_i^{min} \le v_{i,\tau} \le v_i^{max} \tag{14j}$$

where $\Delta SOC_i = SOC_{i,\mathcal{T}_1} - SOC_{i,\mathcal{T}_1+\mathcal{T}-1}$, and $\mathcal{T}_1$ is the initial time of the optimization horizon. The decision variable $\boldsymbol{U}$ is the planned real power for all energy storage devices for the following $\mathcal{T}$-horizon, and $\boldsymbol{\alpha}$ specifies how the energy storage devices partition the aggregate system noise.

E. Noise Modeling and Covariance Computation

In this section, we start with modeling the noise at the lower level, then we derive the upper level noise covariance Σ_τ that is used to construct the chance constraints.

Let vector $W_t \in \mathbb{R}^n$ denote the noise in an n-node distribution system, i.e., $W_t = [w_{1,t}, \ldots, w_{n,t}]^T$, which includes the forecast errors in load and PV generation. Assume

that the noise vector W_t follows a zero-mean Gaussian distribution, i.e., $N(0,\Sigma)$, where the covariance matrix Σ describes the correlation between nodes. To capture the temporal relation and also maintain the stationary property, the noise is modeled in the following Markovian fashion:

$$W_{t+1} = \beta W_t + \sqrt{(1-\beta^2)\Sigma} N_{t+1} \tag{15}$$

where $\beta \in (0,1)$, $W_0 \sim N(0,\Sigma)$, and $N_t \sim \mathcal{N}(0,I)$. The discount factor β specifies the temporal relation between the current and next time steps. Note that β can also be a matrix defining different discount factors for different nodes. For simplicity, we assume that the discount factor is same for all nodes.

Theorem 1. *The n-node noise $W_t \sim N(0,\Sigma)$ for all $t \geq 0$; in addition, its autocovariance matrix:*

$$C_W(k) = \beta^k \Sigma. \tag{16}$$

Proof. Applying the independence between Gaussian random variables W_t and N_{t+1}, the linear combination W_{t+1} is also Gaussian with the following mean and variance:

$$E[W_{t+1}] = \beta E[W_t] + \sqrt{(1-\beta^2)\Sigma}\, E[N_{t+1}] = 0$$

$$\begin{aligned}\Sigma_W &= E[W_{t+1}W_{t+1}^T] - E[W_{t+1}]E[W_{t+1}]^T \\ &= E[W_{t+1}W_{t+1}^T] \\ &= E[\beta^2 W_t W_t^T + (1-\beta^2)\Sigma N_{t+1}N_{t+1}^T] \\ &= \beta^2 \Sigma_W + (1-\beta^2)\Sigma\end{aligned}$$

From the last equation, we obtain that $\Sigma_W = \Sigma$. This completes the proof of $W_t \sim N(0,\Sigma)$.

To compute the autocovariance, we represent W_{t+k} in the following form by using (15):

$$W_{t+k} = \beta^k W_t + \sum_{i=0}^{k-1} \beta^i \sqrt{(1-\beta^2)\Sigma} N_{t+k-i}$$

The autocovariance is computed as:

$$\begin{aligned}C_W(k) &= E[W_{t+k}W_t^T] - E[W_{t+k}]E[W_t]^T \\ &= E[(\beta^k W_t + \sum_{i=0}^{k-1} \beta^i \sqrt{(1-\beta^2)\Sigma} N_{t+k-i})(W_t^T)] \\ &= \beta^k E[W_t W_t^T] + \sqrt{(1-\beta^2)\Sigma} \sum_{i=0}^{k-1} \beta^i E[N_{t+k-i})(W_t^T)] \\ &= \beta^k \Sigma\end{aligned}$$

where the last equation applies the independence between N_{t+s} and W_t, for $s > 0$.

□

Recall that $w_{\Sigma,t}$ is defined as the sum of all node noises at time t, i.e, $w_{\Sigma,t} = \sum_i W_t(i) = e^T W_t$, where $e^T = [1,1,\ldots,1]$.

Corollary 1. *The aggregate noise $w_{\Sigma,t} \sim N(0, e^T\Sigma e)$, and its autocovariance $C_w(k) = \beta^k e^T \Sigma e$.*

The proof is straightforward by using Theorem 1 and the representation $w_t = e^T W_t$.

Corollary 2. *Suppose one time horizon τ in* (14) *contains N time steps, i.e., $\Delta\tau = N\Delta t$, the covariance matrix for the aggregate noise is:*

$$\Sigma_\tau(i,j) = \beta^{N|i-j|} e^T \Sigma e,\ 1 \leq i,j \leq \tau \tag{17}$$

Proof. We first transform the autocovariance from the time index t to τ under the relation $\Delta\tau = N\Delta t$:

$$C_{w_\tau}(k) = C_w(Nk) = \beta^{Nk} e^T \Sigma e$$

The result (17) is then obtained from the fact that:

$$\Sigma_\tau(i,j) = C_{w_\tau}(|i-j|),\ 1 \leq i,j \leq \tau.$$

□

IV. Lower Level Extremum Seeking Control

Solving the upper level OPF problem schedules operations for each energy storage device to minimize the overall energy cost while maintaining sufficient power/energy reserve. This solution, however, might not be optimal because of several factors, including modeling errors in linearized power flow and node noises, and lossless power flow assumption on energy storage and node noises. In addition, the solution provided by (14) addresses $\Delta\tau$ as one time step, whereas the system dynamics are updated much faster than $\Delta\tau$. Given these reasons, we propose adjusting the scheduled energy storage operations according to the feedback from real-time measurements. This objective is accomplished by a control technique named extremum seeking.

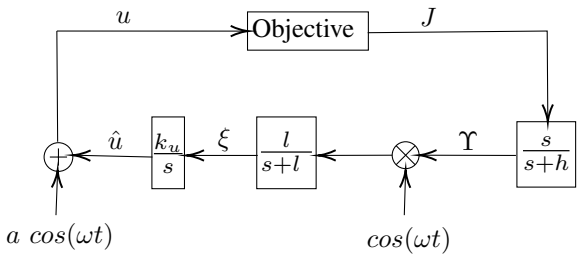

Fig. 2. Extremum seeking control diagram.

Extremum seeking is a model-free optimization technique that optimizes the objective function through real time measurements. It can be viewed as an approximate gradient descent/ascent method. Fig. 2 shows the diagram of a typical ES controller. The goal is to minimize/maximize the objective function $J(u)$, whose mathematical representation is unknown but its real time measurement $J(u_t)$ is available. The gradient is approximated through the modulation signal $a\,cos(\omega t)$, where a is a small constant. To extract the component of J that results from the modulation signal, J is passed through a high-pass filter $s/(s+h)$ to remove its DC component. The obtained signal Υ is then demodulated using signal $cos(\omega t)$. The gradient is approximated by passing Υ through the low-pass filter $l/(s+l)$, and we have $\xi \approx \partial\Upsilon/\partial u$.

Using the obtained gradient, we update the estimate of optimal control $\hat{u}$ through the gradient-based approach: if the gain $k_u < 0\,(k_u > 0)$, the block k_u/s performs as a gradient descent (ascent) method. More details about the ES control can be found in [3].

In this work, the control variable u is the real power of controllable DERs, and the objective function is defined as a squared tracking error:

$$J_t = (P_{1,t} - \bar{P}_{1,t})^2$$

where $\bar{P}_{1,t}$ is the scheduled feeder head power. Note that the objective function value J_t is the same for all DERs, but each controllable DER has a unique ES configuration to control its power output.

The design challenge lies in determining the parameters: a, w, h, l, k. Each local ES controller needs a unique perturbation signal frequency, and $\omega_i + \omega_j \neq \omega_k$, for $i \neq j \neq k$. This allows us to distinguish the contribution of each ES controller during the optimization. The perturbation signal magnitude a should be large enough so that the contribution of the perturbation signal is detectable, but not too large to avoid dragging the input u far from $\hat{u}$. For the high-pass and low-pass filter cutoff frequencies h and l, it is necessary to ensure that the perturbation is not washed out by the high-pass filter but attenuated by the low-pass filter, i.e., $l < \omega$ and $h < \omega$. To minimize the objective function, the integrator gain k_u is negative.

V. Bridging Two-layer Controls

As shown in Fig. 1, the upper and lower level controllers are operated in different timescales. Techniques to properly integrate these two layer controllers are presented in this section.

A. Model Predictive Control

The OPF (14) provides control solutions for the next $\mathcal{T}$ horizons. As time advances, the updated system information and forecasts become available. In this regard, we apply MPC in the following steps: suppose we want to solve the problem for the next T time horizons:

1) Initialize $\mathcal{T}_1 = 1$;
2) Collect current system information and future forecasts over the horizon $\mathcal{T}$;
3) Solve problem (14) and broadcast $\{U_{i,\mathcal{T}_1}, \alpha_{i,\mathcal{T}_1}\}$ to storage i, for each i;
4) $\mathcal{T}_1 = \mathcal{T}_1 + 1$ and go to 2) until $\mathcal{T}_1 = T$.

Step 3) computes the solution for all the following $\mathcal{T}$ time horizons, but it applies control decisions only for the current time horizon $\mathcal{T}_1$. Then, the forecast horizon is shifted by one time horizon, and system information is updated for the computation of new control decisions.

B. Algorithm Implementation

The overall control procedure that combines the upper level chance-constrained MPC and the lower level ES control is summarized in Algorithm 1. Lines 1–4 implement the upper level MPC approach, and lines 5–8 implement the lower level storage operation, where we assume one upper level time horizon contains N lower level time steps, i.e., $\Delta\tau = N\Delta t$.

Algorithm 1: chance-constrained DER scheduling with extremum seeking control.

1: **for** $\mathcal{T}_1 = 1, \ldots, T$ **do**
2: Collect current system information and forecasts;
3: Solve the chance-constrained OPF problem (14);
4: Broadcast the solution $U_{i,\mathcal{T}_1}$, and $\alpha_{i,\mathcal{T}_1}$ to controllable DER i, for all i;
5: **for** $k = 1, \ldots, N$ **do**
6: $t = N(\mathcal{T}_1 - 1) + k$;
7: **for** Storage $i \in \{1, \ldots, n\}$ **do**
8: **if** $k = 1$ **then**
9: DER power $\mathcal{U}_{i,t} = U_{i,\mathcal{T}_1}$;
10: **else if** $k = 2$ **then**
11: DER power $\mathcal{U}_{i,t} = U_{i,\mathcal{T}_1} + \alpha_{i,\tau}\,\beta\,\tilde{w}_{\Sigma,t-1}$;
12: initialize $J_t = 0, \Upsilon_{i,t} = 0, \xi_{i,t} = 0$;
13: **else**
14: Obtain the objective function value J_t;
15: Update $\mathcal{U}_{i,t}$ from extremum seeking control;
16: **end if**
17: **end for**
18: **end for**
19: **end for**

One critical step in connecting the two control layers is proper initialization of the ES controllers when the upper level schedule is updated. In the scheduler, the total noise compensation is distributed to each energy storage device according to the distribution factor $\alpha_{i,\tau}$; however, the lower level ES controllers are myopic, where only the tracking error at the feeder head is considered. This might lead to a different noise compensation distribution among the energy storage devices and insufficient reserve in the future. To address this problem, we pass both $U_{\mathcal{T}_1}$ and $\alpha_{\mathcal{T}_1}$ to the lower level at the beginning of each time horizon, so that we can initialize the ES controllers near the optimal solution obtained from the upper level. Implementing $\alpha_{\mathcal{T}_1}$ requires information about aggregate system noise $w_{\Sigma,t}$. It is estimated as the difference between the planned and actual results:

$$\tilde{w}_{\Sigma,t} = P_{1,t} - \bar{P}_{1,\mathcal{T}_1} + \sum_i (\mathcal{U}_{i,t} - U_{i,\mathcal{T}_1}) \qquad (18)$$

Because $\tilde{w}_{\Sigma,t}$ in (18) is computable only when the control $\mathcal{U}_{i,t}$ and output $P_{1,t}$ are given. As shown in line 11 of Algorithm 1, we use the noise estimation $\tilde{w}_{\Sigma,t} = \beta\tilde{w}_{\Sigma,t-1}$ (following the noise model (15)) to update the control signal $\mathcal{U}_{i,t}$. Simulation results in Section VI suggest that passing $\boldsymbol{\alpha}$ to initialize lower level ES control is crucial to the success of the proposed algorithm.

Line 12 of Algorithm 1 provides another part of initialization for ES control. The intention is to clear the memory of the measurements and internal variables that are not caused by the ES input. After these steps of initialization, ES control is used to track the scheduled feeder head power.

VI. Simulation Study

A. Simulation Setup

Numerical experiments were conducted on a modified IEEE 13-node feeder [18] to test the performance of the proposed approach, and results are presented in this section.

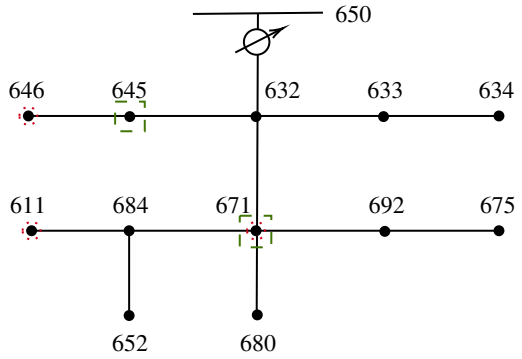

Fig. 3. Modified IEEE 13-node test feeder: PV and energy storage locations are labeled by dots and dashed squares, respectively.

Fig. 3 shows the modified IEEE 13-node test feeder, where three PV systems were added at nodes 646, 671, and 611, and two energy storage devices were added at nodes 645 and 671. Table I provides the configuration of these DERs. The voltage and power base values considered were 4.16 kV and 0.5 MVA, respectively. The feeder head voltage was 1.03 $p.u.$ in the simulations.

TABLE I

Configuration of DERs (per unit).

Node	PV generation	Storage limits	
		SOC	Power
611	$0.3 + 0.2i$	N/A	
645	N/A	[0 1]	[-1 1]
646	$0.16 + 0.1i$	N/A	
671	$0.2 + 0.12i$	[0 1]	[-1.5 1.5]

Noises at the load and PV nodes were generated using (15) with $\beta = 0.9996$, corresponding to the simulation time step $\Delta t = 1$ second. Considering the temporal correlation in the node noises, we constructed the covariance matrix Σ so that closer nodes have a higher correlation. Fig. 4 shows a realization of the noise signal. The forecast horizon is 2 hours, and $\Delta\tau$ = 10 minutes in the upper level OPF planning. Fig. 5 shows the 4-hour electricity price signal used in the simulation, where the last 2-hour prices were used as future information for the MPC.

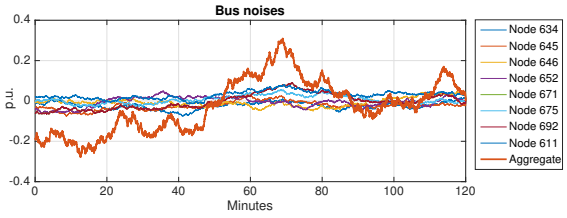

Fig. 4. One example of the noise signal.

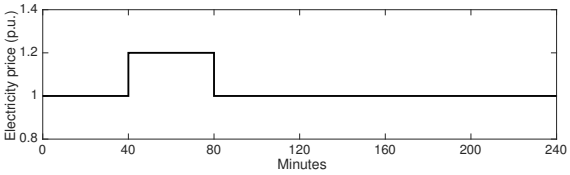

Fig. 5. Electricity price signal.

Two ES controllers for energy storage devices at node 645 and 671 were configured as shown in Table II.

TABLE II

Extremum seeking control parameters.

Node	f(Hz)	h(rad/s)	l(rad/s)	k_u	a (p.u.)
645	0.2	0.0001	0.1	-15	0.004
671	0.17	0.0001	0.1	-15	0.004

B. Simulation Results

In this section, we present the simulation results for several scenarios with different control algorithms. We first studied the control performance when system uncertainty was not considered in the planning ($\Sigma_\tau = 0$) but appeared in the simulation. Then we tested different information exchanges between the two control levels. Finally, we added the MPC to further improve the robustness of the algorithm.

The dashed lines in Fig. 6 show the planning results without considering the system uncertainty. Driven by the cost-saving intent, energy storage devices were scheduled to precharge in the first 40 minutes and then to discharge using their max power during the high-price time period. For 80–120 minutes, the storage devices were scheduled to charge again because the price was lower than the average price. This resulted in no reserve of storage power/energy, and the system is vulnerable to the noise. The solid lines

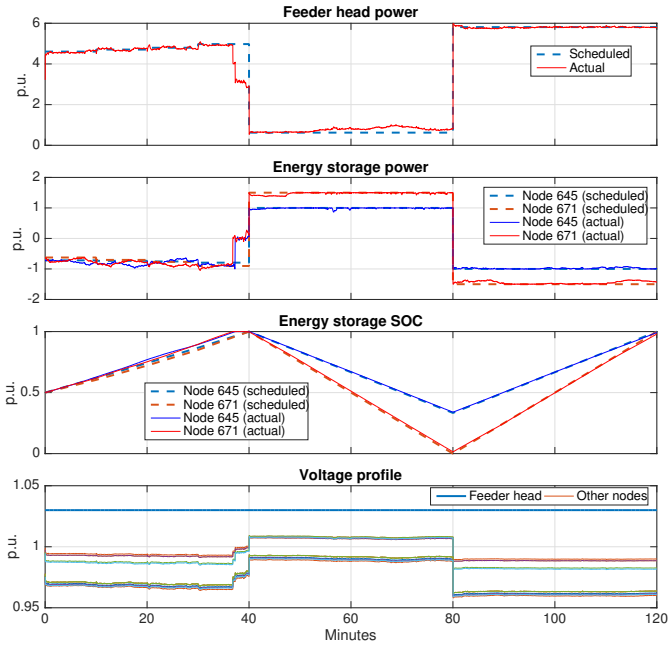

Fig. 6. Power planning (no chance constraints) and tracking results.

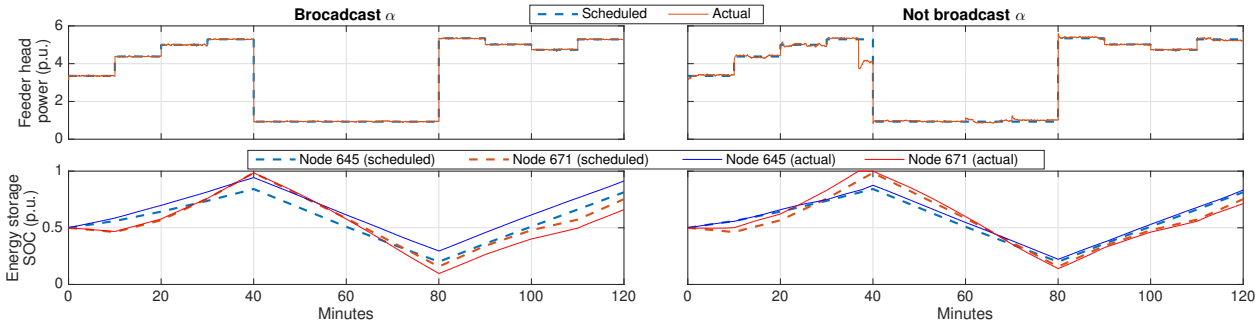

Fig. 7. Chance-constrained power planning and tracking results with and without broadcast the noise distribution factor $\boldsymbol{\alpha}$ to lower level ES controllers, in regard to the noise signal in Fig. 4.

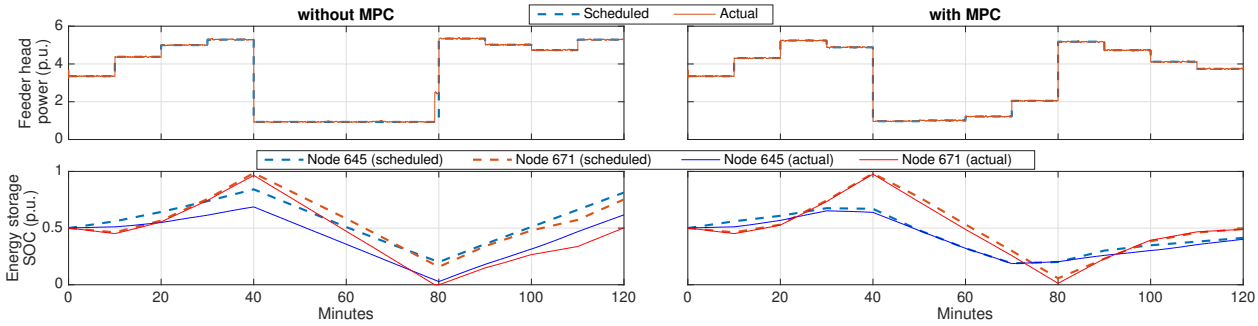

Fig. 8. Chance-constrained power planning and tracking results with and without MPC, in regard to the noise in Fig. 9.

in Fig. 6 show the actual results when the noise signal in Fig. 4 was considered. To compensate for the negative noise injection, the energy storage devices were fully charged before the scheduled time $t = 40$ minutes and then failed to consume the scheduled power, which resulted in a large feeder head power mismatch. During 40–80 minutes, because both energy storage devices were operated at their max discharge power, they were unable to compensate for the positive noise injection.

The planning results with chance constraints included are presented as dashed lines in Fig. 7, where the reliability factor $\gamma = 0.99$. We studied two scenarios distinguished by whether the noise distribution factor $\boldsymbol{\alpha}$ was broadcast to the lower level controllers. The plots on the left-hand-side show the results when the $\boldsymbol{\alpha}$ information was available to lower level controllers. In the planning results, energy storage devices were not scheduled to charge/discharge fully because of the reserve requested by the proposed chance constraints. This strategy resulted in the feeder head power shown as the dashed line in the top-left of Fig. 7. Results against the stochastic noises (Fig. 4) are presented as solid lines. With the help of the storage reserve, the scheduled feeder head power was well tracked. The resulting node voltages are similar to those shown on the bottom of Fig. 6. Because of space limitation, they are not presented.

Results when the noise distribution parameter $\boldsymbol{\alpha}$ was not broadcast to the energy storage devices are shown on the right-hand-side of Fig. 7. Without information about $\boldsymbol{\alpha}$, the energy storage devices managed the system noise merely by the ES control, and the long-term performance will be degraded because the ES optimizes the objective function without looking into the future. As shown in Fig. 7, one storage device was fully charged before $t = 40$ minutes and became unavailable to consume power from the grid. Because of insufficient controllable power capacity, the scheduled feeder head power was not well tracked until the storage devices were requested to supply power after $t = 40$ minutes. In addition, missing information of $\boldsymbol{\alpha}$ made it difficult to properly initialize the ES controllers (recall line 11 of Algorithm 1) and took longer to track the scheduled feeder head power.

All above simulation results are based on the one-time planning solutions through (14), without MPC. We next consider the MPC framework (Algorithm 1) that regularly updates the storage states and price signals at each upper level time step. To compare the performance with and without MPC, the atypical noise signal in Fig. 9 was used in the simulation. This noise remains positive and would request that energy storage devices provide more power than scheduled values.

The left-hand-side of Fig. 8 shows results without MPC. When $t \approx 78$ minutes, the storage at node 671 ran out of energy and failed to supply power. This resulted in a nearly 1.5 $p.u.$ power shortage during 78–80 minutes. When MPC was applied, it updated the system information every 10 minutes and was able to adjust the scheduled controls. As shown on the right-hand-side of Fig. 8, when MPC was performed at $t = 70$ minutes, it reduced the power injection from the energy storage devices, and instead it requested that amount of power from the feeder head.

The reliability parameter γ determines the success rate only for a single chance constraint. Considering that the distribution system consists of multiple constraints that evolve

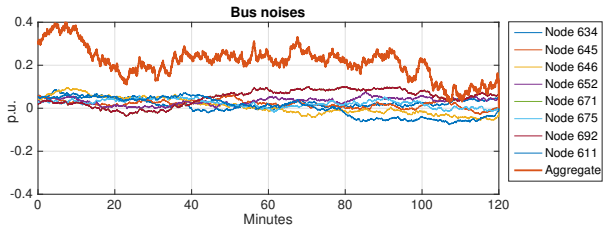

Fig. 9. A noise signal used in MPC simulation.

with time, the joint success rate is likely less than that of a single constraint. To quantify the performance, we consider two metrics: namely, success event rate and feeder head power tracking root mean square error (RMSE). We define a successful event based on two criteria: voltage limits ($[0.95\ 1.05]\,p.u.$) and feeder tracking error ($< 5\%$ for the entire 2-hour simulation), where the tracking error is defined as the percentage of the feeder head baseline power 3.22 $p.u.$

Table III summarizes the success rate and RMSE for different scenarios, where each was tested with 1000 simulation runs that were distinguished by system noises. The algorithm scenario is named in the '*A* + *B*' form, where '*A*' describes the algorithm used in the upper level OPF, and '*B*' describes the information broadcast to the ES controllers. In the table, *CC* refers to the chance-constrained OPF with $\gamma = 0.99$; *MPC* refers to the MPC-based *CC*; *No CC/MPC* refers to the OPF without chance constraints; $\boldsymbol{U}$ and $\boldsymbol{\alpha}$ are corresponding OPF solutions and $\bar{\boldsymbol{\alpha}} = [0.5\ 0.5]^T$ is a flat noise distribution.

TABLE III
COMPARISON OF DIFFERENT ALGORITHM SETTINGS

Scenario	**Success rate**	**RMSE** ($p.u.$)
No CC/MPC + $\boldsymbol{U}$	0.1%	0.2222
CC + $\boldsymbol{U}$	4.2%	0.0873
CC + $\{\boldsymbol{U}, \bar{\boldsymbol{\alpha}}\}$	58.9%	0.0521
CC + $\{\boldsymbol{U}, \boldsymbol{\alpha}\}$	95.6%	0.0179
MPC+ $\{\boldsymbol{U}, \boldsymbol{\alpha}\}$	96.4%	0.0162

The MPC-based approach (Algorithm 1) achieved a 96.4% success rate and 0.0162 $p.u.$ RMSE, which is the best performance among all algorithms considered. The scenarios '*No CC/MPC* + $\boldsymbol{U}$' and '*CC* + $\boldsymbol{U}$' have extreme low success rates because the magnitudes of noise signals are usually larger than the 5% tracking error threshold and the local ES controllers lack the noise distribution strategy $\boldsymbol{\alpha}$. Using the flat noise distribution factor $\bar{\boldsymbol{\alpha}}$ improves the performance, but the results are still far from satisfactory. The last two rows of Table III show good results when both the upper level solutions $\boldsymbol{U}$ and $\boldsymbol{\alpha}$ are broadcast to the ES controllers.

VII. Conclusions and Future Work

In this work, we proposed a hierarchical control architecture for distribution systems. At the upper level, a finite horizon chance-constrained OPF formulation is developed to minimize energy cost and address system uncertainty. At the lower level, the ES control is applied to controllable DERs to meet predetermined OPF schedules under a noisy environment. The proposed hierarchical control is demonstrated on a modified IEEE 13-node test feeder.

The relation between the individual reliability factor γ and the joint success rate has been studied in simulation, but the analytical solution remains an open question. It will be investigated in future work.

Another future research direction is to extend current work to broader DERs with controllable real and reactive power for both feeder head power tracking and voltage control.

References

[1] J. M. Guerrero, F. Blaabjerg, T. Zhelev, K. Hemmes, E. Monmasson, S. Jemei, M. P. Comech, R. Granadino, and J. I. Frau, "Distributed generation: Toward a new energy paradigm," *IEEE Industrial Electronics Magazine*, vol. 4, no. 1, pp. 52–64, 2010.

[2] A. Q. Huang, M. L. Crow, G. T. Heydt, J. P. Zheng, and S. J. Dale, "The future renewable electric energy delivery and management (freedm) system: The energy internet." *Proceedings of the IEEE*, vol. 99, no. 1, pp. 133–148, 2011.

[3] K. Ariyur and M. Krstic, *Real-Time Optimization by Extremum-Seeking Control*, ser. Wiley-interscience publication. Wiley, 2003.

[4] D. Pudjianto, C. Ramsay, and G. Strbac, "Virtual power plant and system integration of distributed energy resources," *IET Renewable Power Generation*, vol. 1, no. 1, pp. 10–16, 2007.

[5] F. Capitanescu, J. M. Ramos, P. Panciatici, D. Kirschen, A. M. Marcolini, L. Platbrood, and L. Wehenkel, "State-of-the-art, challenges, and future trends in security constrained optimal power flow," *Electric Power Systems Research*, vol. 81, no. 8, pp. 1731–1741, 2011.

[6] G. C. Calafiore and M. C. Campi, "The scenario approach to robust control design," *IEEE Transactions on Automatic Control*, vol. 51, no. 5, pp. 742–753, 2006.

[7] F. Bouffard and F. D. Galiana, "Stochastic security for operations planning with significant wind power generation," in *Power and energy society general meeting-conversion and delivery of electrical energy in the 21st century, 2008 IEEE*. IEEE, 2008, pp. 1–11.

[8] D. Bienstock, M. Chertkov, and S. Harnett, "Chance-constrained optimal power flow: Risk-aware network control under uncertainty," *Siam Review*, vol. 56, no. 3, pp. 461–495, 2014.

[9] M. Vrakopoulou, K. Margellos, J. Lygeros, and G. Andersson, "A probabilistic framework for reserve scheduling and N-1 security assessment of systems with high wind power penetration," *IEEE Transactions on Power Systems*, vol. 28, no. 4, pp. 3885–3896, 2013.

[10] E. DallÁnese, K. Baker, and T. Summers, "Chance-constrained ac optimal power flow for distribution systems with renewables," *IEEE Transactions on Power Systems*, vol. 32, no. 5, pp. 3427–3438, 2017.

[11] L. Roald and G. Andersson, "Chance-constrained ac optimal power flow: Reformulations and efficient algorithms," *IEEE Transactions on Power Systems*, vol. 33, no. 3, pp. 2906–2918, 2018.

[12] Y. Lin, J. L. Mathieu, and J. X. Johnson, "Stochastic optimal power flow formulation to achieve emissions objectives with energy storage," in *Power Systems Computation Conference (PSCC), 2016*. IEEE, 2016, pp. 1–7.

[13] B. A. Robbins, C. N. Hadjicostis, and A. D. Domínguez-García, "A two-stage distributed architecture for voltage control in power distribution systems," *IEEE Transactions on Power Systems*, vol. 28, no. 2, pp. 1470–1482, 2013.

[14] N. Li, G. Qu, and M. Dahleh, "Real-time decentralized voltage control in distribution networks," in *Communication, Control, and Computing (Allerton), 2014 52nd Annual Allerton Conference on*. IEEE, 2014, pp. 582–588.

[15] H. Xin, Z. Qu, J. Seuss, and A. Maknouninejad, "A self-organizing strategy for power flow control of photovoltaic generators in a distribution network," *IEEE Transactions on Power Systems*, vol. 26, no. 3, pp. 1462–1473, 2011.

[16] D. B. Arnold, M. Negrete-Pincetic, M. D. Sankur, D. M. Auslander, and D. S. Callaway, "Model-free optimal control of var resources in distribution systems: An extremum seeking approach," *IEEE Transactions on Power Systems*, vol. 31, no. 5, pp. 3583–3593, 2016.

[17] M. Baran and F. F. Wu, "Optimal sizing of capacitors placed on a radial distribution system," *IEEE Transactions on Power Delivery*, vol. 4, no. 1, pp. 735–743, Jan 1989.

[18] W. H. Kersting, *Distribution system modeling and analysis*. CRC press, 2006.